Destruction and resurgence of the quasiperiodic shearless attractor

R. Simile Baroni [*] and R. Egydio de Carvalho [†]

Universidade Estadual Paulista–UNESP, Instituto de Geociências e Ciências Exatas–IGCE, Departamento de Estatística, Matemática Aplicada e Ciências da Computação, Rio Claro-SP 13506-900, Brazil

(Received 21 April 2021; accepted 21 June 2021; published 12 July 2021)

We consider a dissipative version of the standard nontwist map. It is known that nontwist systems may present a robust transport barrier, called shearless curve, that gives rise to an attractor that retains some of its properties when dissipation is introduced. This attractor is known as shearless attractor, and it may be quasiperiodic or chaotic depending on the control parameters. We describe a route for the destruction and resurgence of the quasiperiodic shearless attractor by analyzing the manifolds of the unstable periodic orbits (UPOs) which are fixed points of the map. We show that the shearless attractor is destroyed by a collision with the UPOs and it resurges after the reconnection of the unstable manifolds of different UPOs.

DOI: 10.1103/PhysRevE.104.014207

I. INTRODUCTION

Two-dimensional area preserving maps are great tools for studying transport properties of physical systems, usually described by a Hamiltonian formulation. A well-known example of such models is the twist standard map, which shows the general dynamics of nearly integrable Hamiltonian systems, as described by the KAM (Kolmogorov, Arnold, Moser) and Poincaré-Birkhoff theorems. For a given Hamiltonian function described in action angle variables (I, φ), a necessary condition for the KAM theorem to be valid, is the nondegeneracy condition $\frac{\partial^2 H(\mathrm{I})}{\partial^2 \mathrm{I}} \neq 0$, which is named the twist condition for maps. There is a class of maps that violate this condition, which are called nontwist maps, and they can present the characteristic of exhibiting more than one invariant curve, or periodic orbit, with the same rotation number. The periodic orbits induce isochronous resonances [1], which are visualized in the phase space as twin chains of islands. This degeneracy causes topological rearrangements in the phase space that are unique in nontwist systems, for instance, separatrices reconnection, meandering tori, and the presence of the shearless invariant tori, which represents a robust transport barrier. There are many applications of nontwist systems, as, for instance, the modeling of magnetic field lines in plasma confinement devices with reversed magnetic shear [2–5] and atmospheric zonal flow [6,7].

The generic characteristics of nontwist systems can be observed in the standard nontwist map (SNM), introduced in the context of Rossby waves in shear flow [7]. In the past decades, the SNM has been used for both numerical and analytical investigations regarding transport properties in conservative systems [8–11]. Other versions of the SNM have also been proposed, such as the labyrinthic standard nontwist map (LSNM) [12], which may present many shearless transport barriers.

Conservative systems preserve area in phase space and when dissipation is introduced the systems start to have contracting areas, so that any initial condition (IC) converges to asymptotic states called attractors, which can be regular or chaotic. Chaotic attractors can undergo sudden and qualitative changes as a system parameter is varied. In [13,14] the authors showed that those changes occur when the chaotic attractor collides with an *unstable periodic orbit* (UPO) (or equivalently, collides with the UPO stable manifold). Such events are called crises and have been observed in many experimental setups [15–19]. Different types of crises can be identified depending on the types of changes the chaotic attractor will undergo. The two most common types are (i) boundary crisis, when the chaotic attractor is suddenly destroyed after colliding with a UPO on its basin boundary, and (ii) interior crises, when there is a sudden enlargement of the chaotic attractor after it collides with a UPO in the interior of its basin of attraction.

The effects of dissipation on the shearless barriers have been initially considered in [20]. As stated in Refs. [20–22], when dissipation is considered the shearless curve becomes an attractor on a torus, which was called shearless attractor (SA). The SA may be quasiperiodic or chaotic, depending on the control parameters, and two routes to chaos have been recently reported [21].

In this work we consider the dissipative SNM, in a scenario in which the SA is quasiperiodic, and we rewrite the map equations in order to control the positions of the fixed points of the map. For the parameters we select, there are four fixed points: two UPOs and two attractors, all of period 1. We show that one branch of the unstable manifolds of each UPO accumulates at the SA and that the SA is destroyed when it collides with a UPO, in a similar fashion as a boundary crisis for a chaotic attractor. We also show that when the manifolds of the UPOs interact similarly to the separatrix reconnection, in the conservative case, the SA reappears. The

[*] Corresponding author: r.baroni@unesp.br
[†] ricardo.egydio@unesp.br

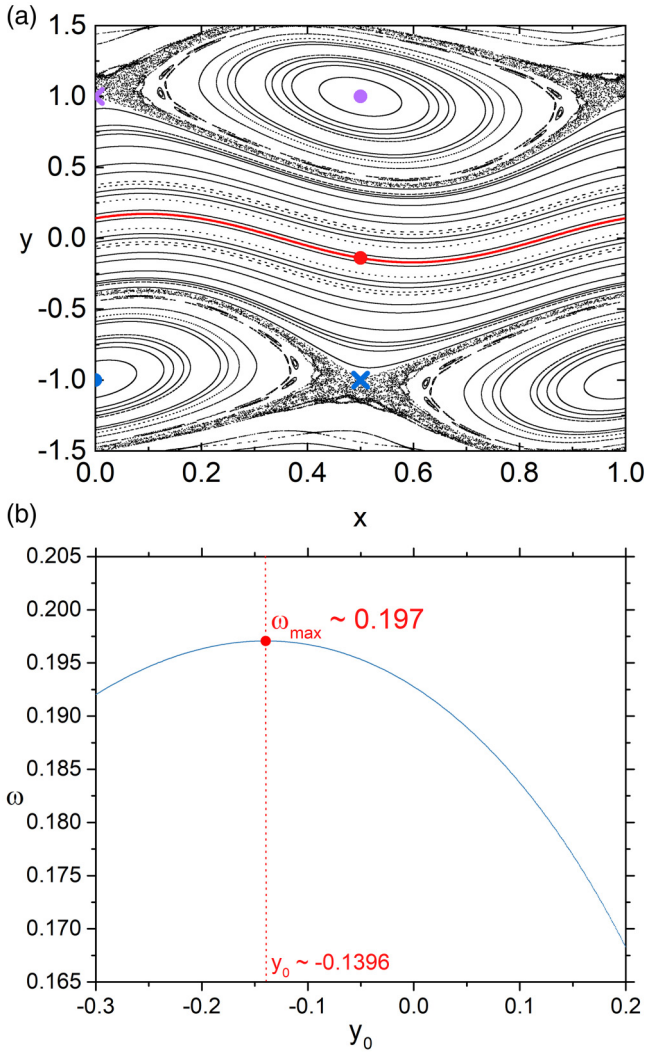

FIG. 1. (a) Phase space of the SNM for $a = 0.2$ and $b = 0.2$. The red curve is the shearless torus. The red point is the initial condition $(x_0, y_0) = (0.5, -0.1396)$, while the purple and blue dots correspond to elliptic fixed points and the blue and purple crosses to hyperbolic fixed points. (b) Rotation number using $x_0 = 0.5$ and $y \in [-0.3,\ 0.3]$. The red dot has $y_0 \sim -0.1396$, which is the coordinate of the extremum. It corresponds to the red point in (a).

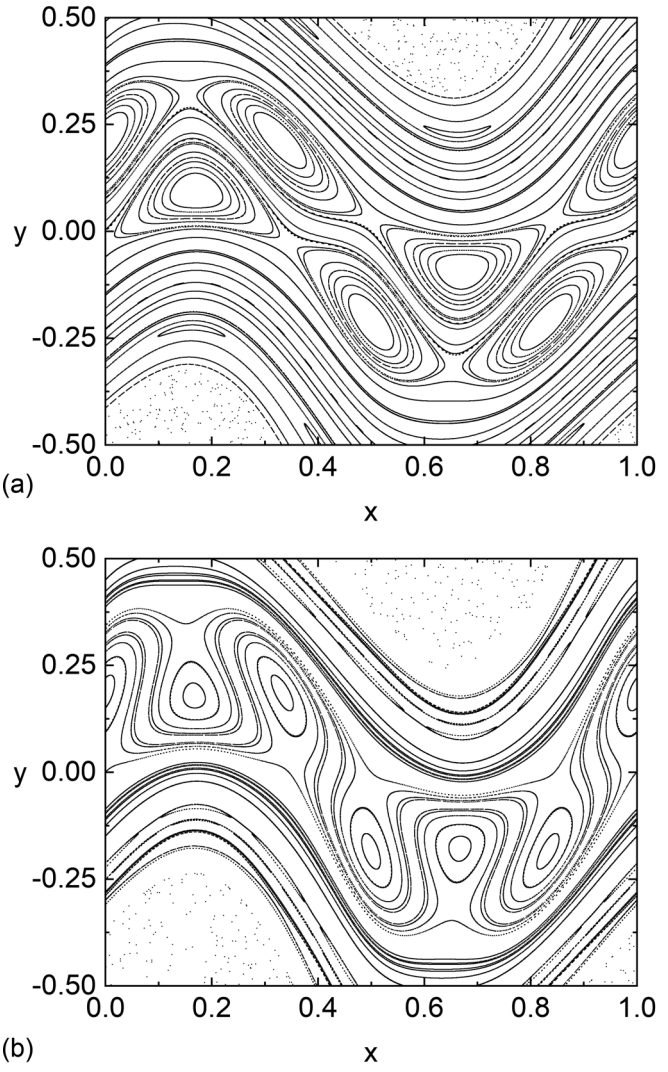

FIG. 2. Phase space illustrating the reconnection process in the SNM for $a = 0.345$ and (a) $b = 0.350$, before the reconnection, and (b) $b = 0.420$ after the reconnection.

paper is organized as follows, in Sec. II we briefly show the main characteristics of the conservative SNM, while in Sec. III we introduce dissipation and abbreviate the map as DSNM; we also present some of its properties and the SA. In Sec. IV the results are presented, and the paper is concluded in Sec. V.

II. BASIC CHARACTERISTICS OF THE STANDARD NONTWIST MAP

The simplest form for the SNM is written as

$$y_{n+1} = y_n - b\sin(2\pi\ x_n), \tag{1}$$

$$x_{n+1} = x_n + a\left(1 - y_{n+1}^2\right), \tag{2}$$

where $y_n \in \mathbb{R}$ and $x_n \in [0,\ 1]$ are canonical variables. The parameter b controls the nonlinearity of the system and a is responsible for the nontwist effects. The nondegeneracy condition, or the so-called twist condition for maps, is violated when $|\frac{\partial x_{n+1}}{\partial y_n}| = 0$ along a curve in the phase space. Consequently, the isochronous resonances emerge in the phase space. The quantity ω is the rotation number and it can be numerically estimated from

$$\omega = \lim_{n\to\infty} \frac{x_n - x_0}{n}, \tag{3}$$

where the variable x is unbounded. The rotation number characterizes the invariant curves in regions of the phase space and its global profile allows us to obtain information about the existence of the robust shearless barrier. The coordinates of the extrema of the rotation number identify a point over the shearless curve. In Fig. 1(a) we illustrate the conservative phase spaces for $a = 0.2 = b$. We note the isochronous resonance islands at $y = \pm 1$ surrounded by stochastic layers. We see a set of invariant spanning curves as well around $y = 0$ and also the shearless curve, which is drawn in red amid them. The red dot has the coordinates $(x,\ y) = (0.5, -0.1396)$ and represents the initial condition that was iterated to generate the

shearless curve. In Fig. 1(b) we exhibit the rotation number profile along the line $x_0 = 0.5$ and the range $y \in [-0.3,\ 0.3]$. We divided this range in 1000 steps and each pair (x_0, y) was iterated $n = 1000$ times through Eqs. (1) and (2); next we executed Eq. (3) to have a point in Fig. 1(b). The red circle in Fig. 1(b) corresponds to a maximum of the rotation number whose coordinates are the IC used in Fig. 1(a).

In Fig. 2 we illustrate the reconnection of the separatri ces, for odd-period orbits, and the meandering tori with $a = 0.345$ and some values of b. As the perturbation is increased, the twin islands' chains approach each other and their size increases. In Fig. 2(a), for $b = 0.350$, we see the scenario before the reconnection of the resonances; in Fig. 2(b), for $b = 0.420$, we see that, after reconnection, the separatrix of the lower UPO looped the upper elliptic fixed point, and vice versa. We also see in Fig. 2(b) the meandering tori, which are invariant curves that are not functions because for a given x there is more than one value of y on the same curve.

III. DISSIPATIVE STANDARD NONTWIST MAP

A dissipative version of the SNM is defined as

$$y_{n+1} = (1-\gamma)\, y_n - b\sin(2\pi x_n), \tag{4}$$

$$x_{n+1} = x_n + a\left(1 - y_{n+1}^2\right), \tag{5}$$

where γ is responsible for the intensity of the dissipation. For $\gamma = 0$ we recover the area preserving dynamics of the SNM. For $0 < \gamma < 1$ the map is area contracting and is called *dissipative standard nontwist map* (DSNM). For the purpose of the analysis that we are going to develop it is convenient to rewrite Eq. (5), so that the DSNM, defined as M_D, is

$$M_D : \begin{cases} y_{n+1} = (1-\gamma)y_n - b\sin(2\pi x_n) \\ x_{n+1} = x_n - a(y_{n+1} - r_1)(y_{n+1} - r_2) \end{cases}, \tag{6}$$

where r_1 and r_2 are the location where two isochronous resonance islands will appear in the nondissipative phase space. Choosing $r_1 = 1$ and $r_2 = -1$ we recover Eq. (5) of the map where the main resonances are located at $y = 1$ and $y = -1$.

The fixed points of the DSNM (x^*, y^*) are obtained by solving the system

$$y^* = (1-\gamma)y^* - b\sin(2\pi x^*), \tag{7}$$

$$x^* = x^* - a({y^*}_{n+1} - r_1)({y^*}_{n+1} - r_2), \tag{8}$$

whose solutions are

$$P_{1,2} = (y^*_{1,2},\ x^*_{1,2}) = \left[r_{1,2},\ \frac{1}{2\pi}\sin^{-1}\left(-\frac{\gamma}{b}r_{1,2}\right)\right]. \tag{9}$$

If $r_1 = -r_2$ the cylindrical symmetry of the map is preserved, and it can be used to find the coordinates of two other symmetric fixed points. A transformation T is said to be a symmetry of the DSMN if $T \circ M_D = M_D \circ T$ holds; then the map is invariant under T. The symbol $\circ$ represents the composition of the maps. It can be easily shown that the DSNM has the following symmetry transformation [23–25],

$$S : \begin{cases} y_{n+1} = -y_n \\ x_{n+1} = x_n \pm \frac{1}{2} \end{cases}; \tag{10}$$

that is, $S \circ M_D = M_D \circ S$, since

$$S \circ M_D : \begin{cases} y_{n+1} = -[\,(1-\gamma)y_n - b\sin(2\pi x_n)] = -(1-\gamma)y_n + b\sin(2\pi x_n) \\ x_{n+1} = x_n - a(y_{n+1} - r_1)(y_{n+1} - r_2) \pm \frac{1}{2} \end{cases}, \tag{11}$$

and

$$M_D \circ S : \begin{cases} y_{n+1} = (1-\gamma)(-y_n) - b\sin\left(2\pi\left(x_n \pm \frac{1}{2}\right)\right) = -(1-\gamma)y_n + b\sin(2\pi x_n) \\ x_{n+1} = x_n - a(y_{n+1} - r_1)(y_{n+1} - r_2) \pm \frac{1}{2} \end{cases}. \tag{12}$$

Applying S to $P_{1,2}$ we obtain the coordinates of two other fixed points $SP_{1,2}$:

$$SP_{1,2} \equiv S(y^*_{1,2},\ x^*_{1,2}) = \left[-r_{1,2},\ \frac{1}{2\pi}\sin^{-1}\left(-\frac{\gamma}{b}r_{1,2}\right) \pm \frac{1}{2}\right]. \tag{13}$$

The fixed points are attractors of period 1 or hyperbolic equilibrium points, also referred to as UPOs. The classification is given according to the eigenvalues of the Jacobian matrix at the fixed points.

It is worth mentioning that when $\gamma = 0$ we recover the conservative scenario of Fig. 1, and the elliptic points of the resonance islands are the fixed point P_2, drawn as a blue circle, and the fixed point SP_2, drawn as a purple circle. Similarly, the hyperbolic points are the fixed points P_1 and SP_1.

When dissipation is considered the elliptic fixed points, the shearless curve, and the chaotic sea of the area preserving maps are replaced by attractors. The elliptic fixed points give rise to sinks and it has been shown that the shearless curve becomes the SA, which may be quasiperiodic or chaotic depending on control parameters and the chaotic seas may become chaotic attractors.

The symmetry properties of nontwist maps can be exploited in order to find the shearless curve [10,11]. For $\gamma = 0$, the DSNM can be decomposed in two maps, named I_0 and I_1, so that $M_D = I_0 \circ I_1$. Both I_0 and I_1 are involutions, that is, $I^2_{0,1} = \mathrm{II}$, and they are written as

$$I_0 : \begin{cases} y_{n+1} = y_n - b\sin(2\pi x_n) \\ x_{n+1} = -x_n \pm \frac{1}{2} \end{cases}, \tag{14}$$

$$I_1 : \begin{cases} y_{n+1} = y_n \\ x_{n+1} = -x_n - a(y_{n+1} - r_1)(y_{n+1} - r_2) \end{cases}. \tag{15}$$

The fixed points of I_0 and I_1 define symmetry lines, that are useful in the search of periodic orbits as developed in Refs. [9–11]. The shearless curve is invariant under the transformations $S \circ I_0$ and $S \circ I_1$,

$$S \circ I_0 : \begin{cases} y_{n+1} = -y_n + b \sin(2\pi x_n) \\ x_{n+1} = -x_n \pm \frac{1}{2} \end{cases}, \tag{16}$$

$$S \circ I_1 : \begin{cases} y_{n+1} = -y_n \\ x_{n+1} = -x_n + a(y_{n+1} - r_1)(y_{n+1} - r_2) \pm \frac{1}{2} \end{cases} \tag{17}$$

because of that, the fixed points of those transformations always belong to the shearless curve. Those fixed points are called indicator points (IPs), and we find

$$(\mathrm{IP}_0)_{1,2} = \left(\pm\frac{b}{2}, \pm\frac{1}{4}\right), \tag{18}$$

$$(\mathrm{IP}_1)_{1,2} = \left(0, -\frac{a r_1 r_2}{2} \pm \frac{1}{4}\right). \tag{19}$$

When dissipation is introduced, we expect that the indicator points belong to the basin of attraction of the SA, at least for a range of parameters. In Fig. 3(a) we show the resulting attractors when a weak dissipation, $\gamma = 0.1$, is added. The elliptic fixed points of the isochronous resonance islands become two punctual attractors and the shearless curve becomes a quasiperiodic SA. The coordinates of the point attractors and of the two UPOs are given by the fixed points of the map, given by Eqs. (9) and (11). The coexistence of attractors, as seen here, is known as a multistability scenario. In Fig. 3(b) we calculate the rotation number, through Eq. (3), along the line $y \in [-0.5, 1.0]$ in a similar fashion as was done for Fig 1(b), but discarding the transient to make sure the ICs have converged to an attractor. We see that initially the rotation number is positive and constant along part of the y curve, whose ICs converge to the SA. At some point, around $y_0 \sim 0.63$, it drops to zero, showing that the ICs from that point on converge to the point attractor. We note that the SA has approximately the same rotation number as the shearless curve of the conservative phase space. The indicator points are points that belong to the shearless curve. As shown in Fig. 3, when a weak dissipation is introduced, we obtain a shearless attractor that has a shape similar to the shearless curve of the conservative counterpart. Although the indicator points no longer exist in the dissipative scenario, we expect the coordinates of the (ex-) indicator points to be on the shearless attractor, or close enough to it to be in its basin of attraction. In the next section the indicator points will be used to compute the bifurcation diagram.

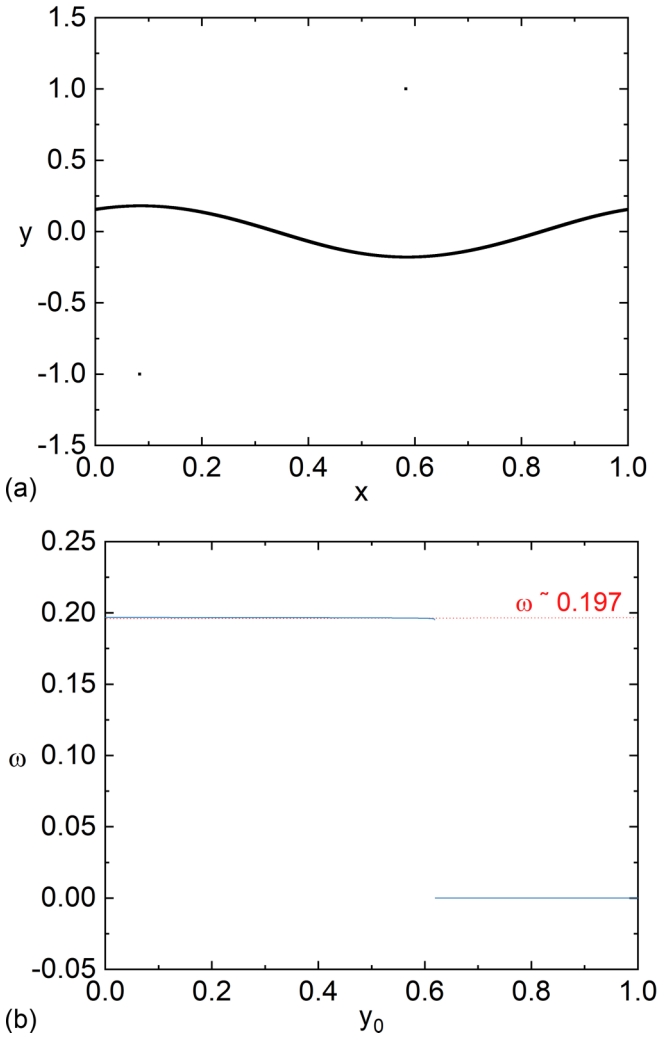

FIG. 3. (a) Attractors of the DSNM for $r_1 = 1.0 = -r_2$, $a = 0.2$, $b = 0.2$, and $\gamma = 0.1$. The invariant curve is the shearless attractor. (b) The rotation number profile using $x_0 = 0.5$ and $y \in [-0.5, 1.0]$. The red dotted line corresponds to the extremum of the rotation number.

IV. RESULTS AND DISCUSSION

We proceed now to vary r_1 and r_2 symmetrically, with $r_2 = -r_1$, in order to approach the sinks P_2 and SP_2, and the UPOs P_1 and SP_1 to the shearless attractor and so to induce topological changes in the phase space. To observe the changes in the profile of the SA, we compute a bifurcation diagram for a fixed set of parameters (a, b, γ). In Fig. 4(a) we choose as IC the indicator point $(\mathrm{IP}_1)_1$, given by Eq. (19), which presumably will be in the basin of attraction of the shearless attractor when dissipation is considered. Then we iterate that IC for a long time and plot the last 2000 values of y for decreasing values of r_1, starting from $r_1 = 1$. We can see that from $r_1 = 1$ to a critical value $r_1 = 0.635\,64$ the IC converges to an attractor that spreads itself over ranges of y values. For values of r_1 between $0.313\,31$ and $0.635\,64$, the IC converges to a point attractor. For a narrow parameter window in that interval, it converges to an attractor with positive y coordinate, but as the parameter changes, the IC converges to another point attractor with a negative y coordinate. For values of r_1 below $0.313\,31$, the IC converges again to an attractor that spreads itself over the y values.

In Fig. 4(b) we plot the value of the largest Lyapunov exponent, λ, of the corresponding orbit shown in the bifurcation diagram, for each value of r_1. The Lyapunov exponent verifies if two neighboring orbits diverge exponentially from each other in time. If the orbits diverge, $\lambda > 0$ and the dynamics

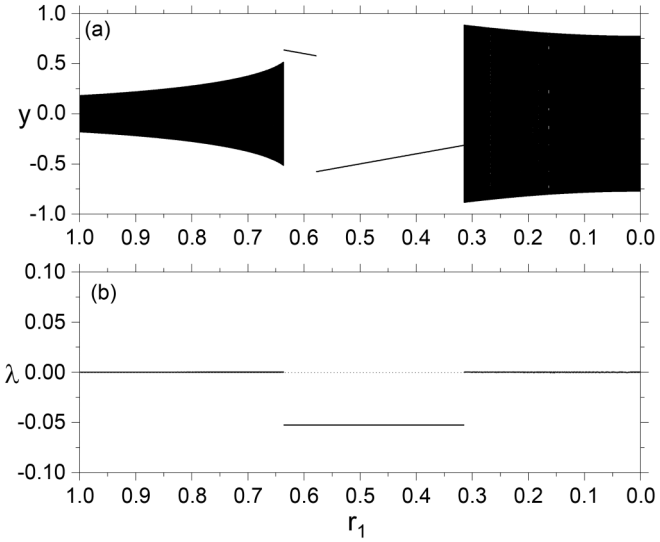

FIG. 4. (a) Bifurcation diagram for $a = 0.2$, $b = 0.2$, and $\gamma = 0.1$; the black points are the last 2000 iterations of the orbit. (b) Lyapunov exponent computed for the orbit in the diagram.

is chaotic. Orbits that stay close to each other result in $\lambda = 0$ or $\lambda < 0$, characterizing quasiperiodic and periodic orbits, respectively. The Lyapunov exponents were calculated according to the Eckmann-Rouelle algorithm [26], defined as

$$\lambda_j = \lim_{n\to\infty}\left\{\frac{1}{n}\ln\left|\Lambda_j^{(n)}\right|\right\}, \quad j = 1, 2, \ldots, \tag{20}$$

where $\Lambda_j^{(n)}$ are the eigenvalues of the matrix $M = \prod_{i=1}^{n} J(x_i, y_i)$, with $J(x_i, y_i)$ being the Jacobian matrix calculated at the point (x_i, y_i).

We see in Fig. 4(b) that the chosen IC shows quasiperiodic behavior, $\lambda = 0$, when the attractor is not pointlike. This attractor is the quasiperiodic SA. In Figs. 5(a) and 5(d) the SA is drawn in red, for $r_1 = 1.0$ and $r_1 = 0.2$. When the SA disappears, λ sharply drops to a negative value, indicating that the IC has collapsed into a periodic attractor.

Associated with every attractor there is the corresponding basin of attraction, which is a region formed by the set of initial conditions that asymptotically reaches the attractor. In Fig. 5 we show three attractors in red: two punctual attractors with coordinates given by the points P_2 and SP_2 of Eqs. (9) and (13), and the SA. We also show their respective basins of attraction for four different values of r_1, keeping $r_2 = -r_1$. For the first one, $r_1 = 1$, we can see in the bifurcation diagram of Fig. 4(a) that the SA exists, and in Fig. 5(a) we see that it coexists with two punctual attractors. They do not appear in the bifurcation diagram because the used IC converged to the SA. The basin of attraction of the SA is shown in gray, while the basins of attraction of the up and down point attractor are shown in green and purple, respectively. We also show the IC used to compute the bifurcation diagram as a blue star, which is over the SA. In Fig. 5(b), for $r_1 = 0.6$, we have a configuration where the SA does not exist and the IC converges to the upper point attractor, as seen in Fig. 4(a) and confirmed by the position of the IC (blue star) in the green

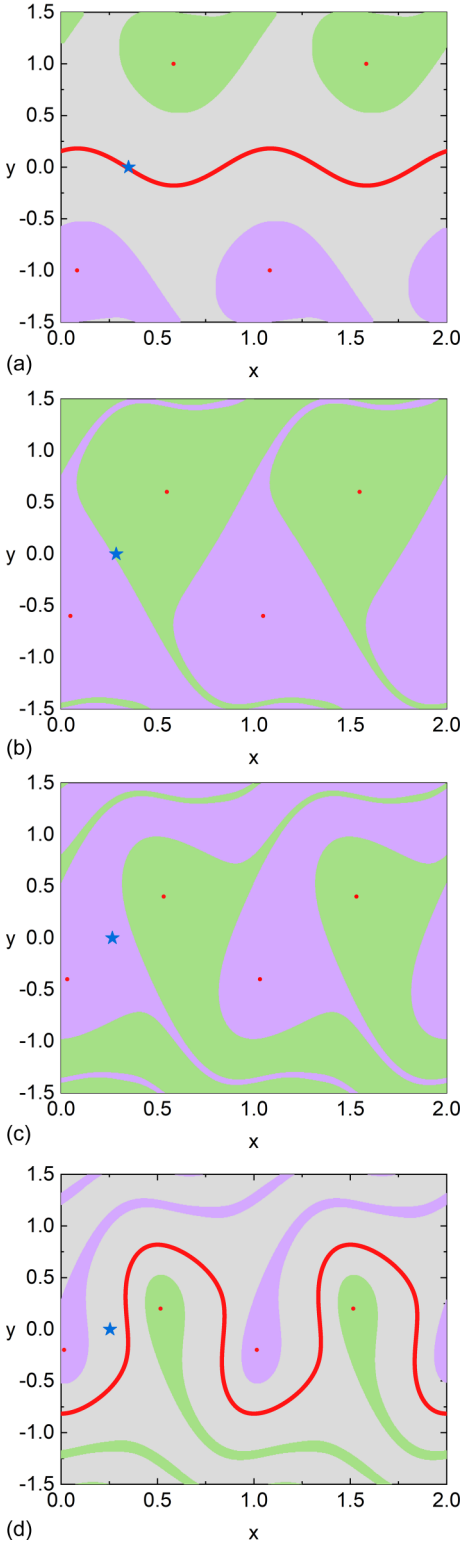

FIG. 5. Attractors of the DSNMs and their basins of attractions for $a = 0.2$, $b = 0.2$, and $\gamma = 0.1$. (a) $r_1 = 1.0$, (b) $r_1 = 0.6$, (c) $r_1 = 0.4$, and (d) $r_1 = 0.2$. In all cases, $r_2 = -r_1$.

basin of attraction. In Fig. 5(c) we use $r_1 = 0.4$. The change of the parameters leads to a rearrangement of the basins of attraction and the IC now converges to the down point attractor. Finally, in Fig. 5(d), we see that the SA is present again; the

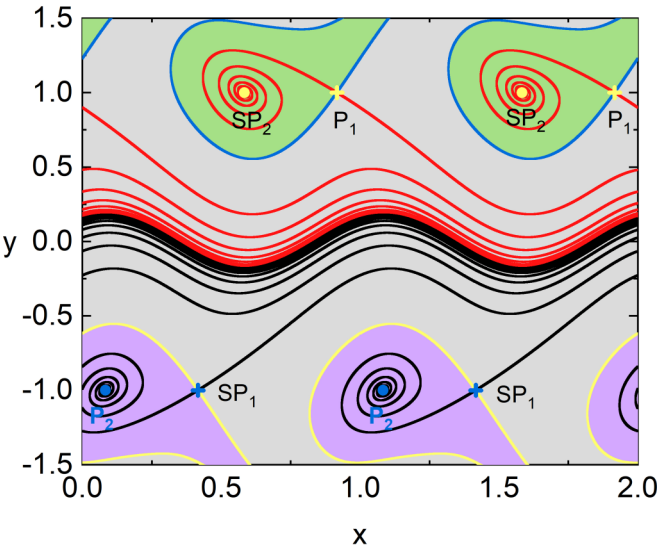

FIG. 6. Basins of attraction of the DSNMs' attractors for $r_1 = 1.0 = -r_2$, a $= 0.2$, $b = 0.2$, and $\gamma = 0.1$.

SA resurged. Even though the IC is not over the SA, it is inside its basin of attraction, so it is possible to see the SA in the bifurcation diagram of Fig. 4(a). Note that we have extended the x-axis range from 0 to 2 to aid the visualization of the basins.

To analyze the mechanism of destruction and resurgence of the SA, we now analyze the role of the fixed points of the map and the corresponding manifolds of the UPOs as r_1 is varied. In Fig. 6 we exhibit the basins of attraction of the attractors of the DSNM for $r_1 = 1$, the same configuration as the one in Fig. 1(b). The point attractors located at P_2 and SP_2 are represented by circles, and the UPOs P_1 and SP_1 by crosses. The unstable (stable) manifold of P_1 is drawn in red (blue). For SP_1, the unstable (stable) manifold is drawn in black (yellow).

Analyzing the unstable manifold of the UPO P_1 we see that one of its branches goes into SP_2's basin of attraction and spirals toward SP_2. The other branch of the unstable manifold goes into the SA's basin of attraction and accumulates over the attractor itself. We also see that the boundary between the basins of attraction of the SA and the periodic attractor is well defined by the stable manifold. The scenario is analogous for the manifolds of the other UPO, at SP_1.

In Fig. 7 we see the basins of attraction and the UPOs manifolds for (a) $r_1 = 0.65$ and (b) $r_1 = 0.6$. As r_1 decreases the basins of attraction of the sinks become larger as they approach the SA. Additionally, as the UPOs approach the SA, we see that the SA bends toward them until it collides simultaneously with both UPOs on the basin boundary (or, equivalently, with the stable manifolds) and is destroyed. After the destruction of the SA, the basins of attraction of the sinks fill the whole space and the boundary between them is defined by the stable manifolds of the UPOs. The UPO's unstable manifolds, which accumulated at the SA, now spiral around the opposite sink. That is, each unstable branch of the manifolds of each UPO spirals toward a different sink.

This mechanism of destruction of the SA is similar to the boundary crises that are observed in systems with a chaotic

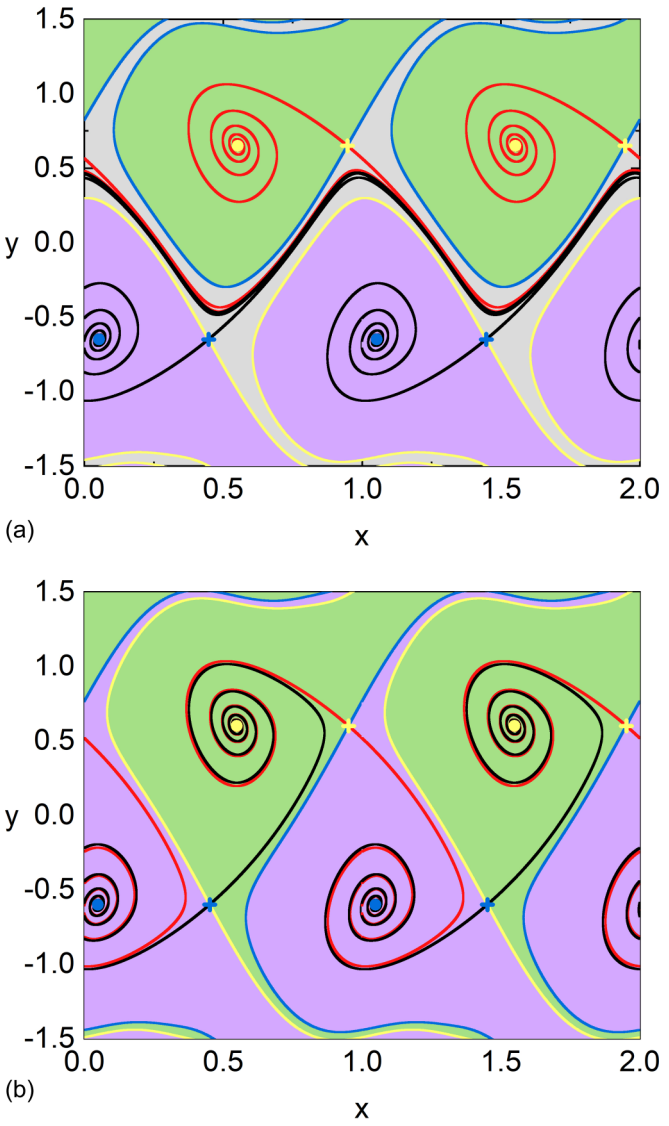

FIG. 7. Basins of attraction of the DSNMs' attractors for $a = 0.2$, $b = 0.2$, and $\gamma = 0.1$. (a) $r_1 = 0.65$ and (b) $r_1 = 0.6$. In all cases, $r_2 = -r_1$.

attractor. A crisis occurs when sudden and qualitative changes happen to a chaotic attractor as a system parameter is varied. Specifically, at a boundary crisis the chaotic attractor collides with a UPO on the basin boundary and is destroyed. The chaotic attractor becomes a nonattracting chaotic set that generates transient chaos. Concerning the SA destruction presented here, no nonattractive chaotic set is created and, therefore, we do not observe any transient chaotic behavior. To illustrate the resurgence mechanism of the SA, as seen in the bifurcation diagram of Fig. 4(a) around $r_1 = 0.30$, we show, in Fig. 8, plots of the point attractors and the UPO's unstable manifolds for decreasing values of r_1. In Fig. 8(a), for $r_1 = 0.65$, we see that the SA (drawn in blue) coexists with two punctual attractors. Decreasing to $r_1 = 0.60$ the SA does not exist anymore because it has collided with the UPOs. Upon decreasing r_1 even further, the upper UPO approaches the branch of the lower UPO's unstable manifold that spirals

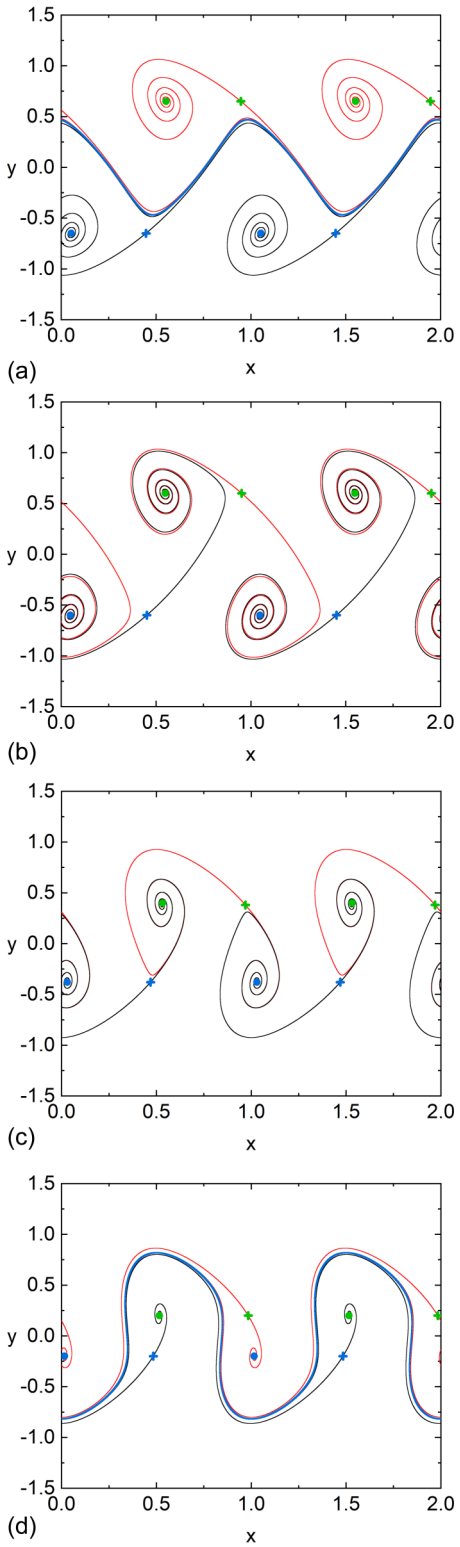

FIG. 8. Stable manifolds of the DSNMs' UPOs for $a = 0.2$, $b = 0.2$, and $\gamma = 0.1$. (a) $r_1 = 0.65$, (b) $r_1 = 0.60$, (c) $r_1 = 0.38$, and (d) $r_1 = 0.20$. In all cases, $r_2 = -r_1$.

into the lower attractor, and the lower UPO approaches the branch of the upper UPO's unstable manifold that spirals into the upper attractor. This is shown in Figs. 8(b) and 8(c), where we kept only the unstable manifolds of the UPOs, fo $r_1 = 0.60$ and $r_1 = 0.38$, respectively. In Fig. 8(d) we choose $r_1 = 0.20$, and we note that the manifolds of the UPOs have interacted, that is, a collision occurred between the saddle point and an unstable manifold, and then a meandering SA appears, drawn in blue. One branch of the unstable manifold spirals into a sink and the other one accumulates on the SA. Thus, the SA reappears after the manifolds of the twin UPOs interact with each other in a similar way to the separatrix reconnection of the conservative counterpart.

V. CONCLUSION

We described a route for the destruction and resurgence of the quasiperiodic shearless attractor. The DSNM was presented in a way that the positions of the fixed points of the map can be controlled as the parameter r_1 is changed, keeping $r_2 = -r_1$ to preserve the symmetry of the map. The fixed points are (i) a period one attractor and a UPO with positive y coordinate equal to r_1, and (ii) a period one attractor and a UPO with negative y coordinate equal to r_2. We analyze the basins of attraction of the point attractors, of the SA, and the behavior of the stable and unstable manifolds of the UPOs. We show that for each UPO, one branch of the unstable manifold goes toward a point attractor while the other one accumulates at the SA. The stable manifolds define the boundaries between the basins of attraction of the periodic attractors and the SA. We compute a bifurcation diagram choosing as initial condition an indicator point of the SNM and we vary r_1. Alongside this diagram we show the Lyapunov exponent of the corresponding orbit in the bifurcation diagram, in order to distinguish between periodic and quasiperiodic behavior. We see that the quasiperiodic SA initially exists but upon decreasing r_1 it is destroyed, and the remaining attractors are the periodic ones. Decreasing r_1 even further shows that the SA reappears. To investigate the mechanism behind this scenario, we analyze the basins of attraction of the attractors and the manifolds of the UPOs. We see that approaching the fixed points to the SA, the basins of attraction of the point attractors grows and the SA bends toward the UPOs. Eventually the SA collides with the UPOs and is destroyed in a similar way to a boundary crisis, in which a chaotic attractor collides with a UPO on the boundary of its basin of attraction. After the destruction of the SA, each branch of the unstable manifold of each one of the UPOs goes into a different point attractor. Approaching the fixed points even further, the unstable manifold of each UPO collides with the opposite UPO, and after this intersection the quasiperiodic SA resurges. This mechanism and these properties allow us to improve the characterization of this attractor.

ACKNOWLEDGMENTS

We acknowledge support from the Brazilian scientific agency CAPES–Coordination for the Improvement of Higher Education Personnel. R.E.C. also thanks CNPQ–National Council for Scientific and Technological Development through Grant No. 306034/2015-8, and FAPESP–São Paulo Research Foundation through Grant No. 2019/07329-4.

[1] R. Egydio de Carvalho and A. M. Ozorio de Almeida, Integrable approximation to the overlap of resonances, Phys. Lett. A **162**, 457 (1992).
[2] P. J. Morrison, Magnetic field lines, Hamiltonian dynamics, and nontwist systems, Phys. Plasmas **7**, 2279 (2000).
[3] J. S. E. Portela, I. L. Caldas, and R. L. Viana, Tokamak magnetic field lines described by simple maps, Eur. Phys. J. Spec. Top. **165**, 195 (2008).
[4] M. Roberto, E. C. Da Silva, I. L. Caldas, and R. L. Viana, Nontwist field line mappings for tokamaks with reversed magnetic shear, Braz. J. Phys. **34**, 1759 (2004).
[5] J. S. E. Portela, I. L. Caldas, R. L. Viana, and P. J. Morrison, Diffusive transport through a nontwist barrier in tokamaks, Int. J. Bif. Chaos **17**, 1589 (2007).
[6] D. Del-Castillo-Negrete, Chaotic transport in zonal flows in analogous geophysical and plasma systems, Phys. Plasmas **7**, 1702 (2000).
[7] D. Del-Castillo-Negrete and P. J. Morrison, Chaotic transport by Rossby waves in shear flow, Phys. Fluids A **5**, 948 (1992).
[8] A. C. Mathias, M. Mugnaine, M. S. Santos, J. D. Szezech, I. L. Caldas, and R. L. Viana, Fractal structures in the parameter space of nontwist area-preserving maps, Phys. Rev. E **100**, 052207 (2019).
[9] A. Wurm, A. Apte, and P. J. Morrison, On reconnection phenomena in the standard nontwist map, Braz. J. Phys. **34**, 1700 (2004).
[10] S. Shinohara and Y. Aizawa, Indicators of reconnection processes and transition to global chaos in nontwist maps, Prog. Theor. Phys. **100**, 219 (1998).
[11] D. Del-Castillo-Negrete, J. M. Greene, and P. J. Morrison, Area preserving nontwist maps: Periodic orbits and transition to chaos, Phys. D (Amsterdam, Neth.) **91**, 1 (1996).
[12] C. G. L. Martins, R. Egydio de Carvalho, I. L. Caldas, and M. Roberto, Labyrinthic standard non-twist map, J. Phys. A: Math. Theor. **44**, 045102 (2011).
[13] C. Grebogi, E. Ott, and J. A. Yorke, Chaotic Attractors in Crisis, Phys. Rev. Lett. **48**, 1507 (1982).
[14] C. Grebogi, E. Ott, and J. A. Yorke, Crises, sudden changes in chaotic attractors, and transient chaos, Phys. D (Amsterdam, Neth.) **7**, 181 (1983).
[15] V. N. Chizhevsky, R. Vilaseca, and R. Corbalán, Amplification of near-resonant signals via stochastic resonance in a chaotic laser, Phys. Rev. E **61**, 6500 (2000).
[16] W. L. Ditto, S. Rauseo, R. Cawley, C. Grebogi, G. H. Hsu, E. Kostelich, E. Ott, H. T. Savage, R. Segnan, M. L. Spano, and J. A. Yorke, Experimental Observation of Crisis-Induced Intermittency and its Critical Exponent, Phys. Rev. Lett. **63**, 923 (1989).
[17] A. S. de Paula, M. A. Savi, and F. H. I. P. Pinto, Chaos and transient chaos in an experimental nonlinear pendulum, J. Sound Vib. **294**, 585 (2006).
[18] M. T. Kitano, T. Yabuzaki, and T. Ogawa, Symmetry-recovering crises of chaos in polarization-related optical bistability, Phys. Rev. A **29**, 1288 (1984).
[19] T. N. Nogueira, F. A. C. Pereira, J. Procopio, and J. C. Sartorelli, Dripping faucet dynamics in a nonuniform electric field, Chaos **28**, 113101 (2018).
[20] R. Egydio De Carvalho and C. V. Abud, Robust attractor of nontwist systems, Physica A **440**, 42 (2015).
[21] M. Mugnaine, A. M. Batista, I. L. Caldas, J. D. Szezech Jr., R. Egydio de Carvalho, and R. L. Viana, Curry–Yorke route to shearless attractors and coexistence of attractors in dissipative nontwist systems, Chaos **31**, 023125 (2021).
[22] L. Kimi Kato and R. Egydio de Carvalho, Transport barriers with shearless attractors, Phys. Rev. E **99**, 032218 (2019).
[23] E. Petrisor, Nontwist area preserving maps with reversing symmetry group, Int. J. Bif. Chaos **11**, 497 (2001).
[24] J. M. Greene, Two-dimensional measure-preserving mappings, J. Math. Phys. **9**, 760 (1968).
[25] R. de Vogelaere, in *Contributions to the Theory of Nonlinear Oscillations*, edited by S. Lefschetz (Princeton University Press, Princeton, NJ, 1958), Vol. IV, p. 53.
[26] J. P. Eckmann and D. Ruelle, The theory of chaotic attractors, in *Ergodic Theory of Chaos and Strange Attractors* (Springer, Berlin, 1985), p. 273.